ARTICLE NO. 78-1361R

Some Effects of Parameter Variations on the Lateral-Directional Stability of Aircraft

Robert F. Stengel*
Princeton University, Princeton, N.J.

Methods of analyzing the effects of aerodynamic uncertainties on the stability of lateral-directional motions are presented. Truncated and "residualized" reduced-order models of the motion are developed. Together with covariance analysis, these models provide simplified estimates of the probability of instability. A Space Shuttle entry flight condition is examined with this technique, and the predicted probability of open-loop instability is found to be low (<0.0001). Monte Carlo stability analysis illustrates that closed-loop control can increase the probability of instability as a consequence of uncertainty in the control derivatives.

Nomenclature

b	= reference length
$C_{l(\ )}, C_{n(\ )}$	= dimensionless aerodynamic derivatives
$\boldsymbol{c}$	= characteristic equation coefficient vector
F	= fundamental (stability) matrix
G	= control effects matrix
g	= gravitational acceleration magnitude
H_B^S	= body-to-stability-axis transformation matrix
I	= identity matrix
I_B	= inertia matrix
I_{xx}, I_{zz}, I_{xz}	= moments and product of inertia
$L_{(\ )}$	= dimensional roll stability and control derivatives
m	= standard deviation multiplier
$N_{(\ )}$	= dimensional yaw stability and control derivatives
P	= parameter covariance matrix
p	= roll rate
$\boldsymbol{p}$	= aerodynamic parameter vector
q	= dynamic pressure
r	= yaw rate
S	= reference area
s	= Laplace operator
V	= velocity magnitude
$\boldsymbol{x}$	= state vector
$Y_{(\ )}$	= dimensional side-force stability and control derivatives
α	= real part of eigenvalue
β	= sideslip angle
$\Delta(s)$	= characteristic equation
$\boldsymbol{\delta}$	= control vector
$\delta R, \delta A$	= rudder and aileron deflections
ζ	= damping ratio
Λ	= eigenvalue covariance matrix
λ	= eigenvalue
μ, ρ	= correlation coefficients
σ	= standard deviation
τ	= time constant
ϕ	= roll angle
ω	= frequency; imaginary part of eigenvalue

Subscripts and Superscripts (other than above)

c	= command
D	= directional
DR	= Dutch roll
F	= fast dynamics
i	= index
L	= lateral
n	= natural
R	= roll mode
S	= spiral mode; also slow dynamics

Received June 20, 1978; presented as Paper 78-1361 at the AIAA 1978 Atmospheric Flight Mechanics Conference, Palo Alto, Calif., Aug. 7-9, 1978; revision received July 2, 1979.

Index categories: Handling Qualities, Stability and Control; Guidance and Control; Aerodynamics.

*Associate Professor of Mechanical and Aerospace Engineering. Associate Fellow AIAA.

Introduction

THE lateral-directional motions of conventional aircraft typically partition into Dutch roll, roll, and spiral modes; these modes provide "weather-cocking" directional stability, damped roll rate response, and a long-term tendency to maintain wings level or to "roll off" in a divergent spiral.[1-3] When the dihedral effect is high and roll damping is low, the roll and spiral modes may coalesce in a single roll-spiral oscillation, or "lateral phugoid" mode. If this is combined with low directional stability and large adverse yaw due to aileron (or elevon), the potential for piloting difficulties may become large. Uncertainties in aerodynamic parameters further increase the risks of mission degradation or failure on early flights of a new aircraft.

To a large extent, known deficiencies in flying qualities can be corrected by the aircraft's flight control system (FCS), but there is, of course, no guarantee that the FCS will properly account for unknown deficiencies. Closed-loop control tends to decrease the sensitivity of system performance to parameter variations, particularly if insensitivity is a design objective.[4] Nevertheless, a given FCS may provide insensitivity to parameter variations of one type at the expense of increased sensitivity to variations of another type. For example, in minimizing performance degradation caused by stability derivative variations, a high-gain controller may inadvertently increase the sensitivity to control derivative variations. In such case, the statistics of the parameter variations, i.e., the probabilities that such variations will occur, are of paramount importance in achieving a "best" FCS design.

This paper presents an analysis of the effects of deterministic and stochastic parameter variations on the lateral-directional stability of an aircraft, using a Space Shuttle dynamic model for numerical examples. Linear dynamic models of lateral-directional motion are reviewed, with the specific objective of developing simple (reduced-order) models of the rigid-body motions. These models provide

insight regarding the basic modes of motion, but more complex models are required to evaluate FCS effects. (One of the quandaries of modern aircraft FCS development is that the classical modes of motion tend to be masked by control compensation.) Higher-order models are used to illustrate the tradeoff between stability- and control-derivative sensitivity, and a technique for evaluating the probability of instability by Monte Carlo computation of eigenvalues is presented.

Dynamic Equations

The coupled dynamics of small lateral-directional perturbations typically are described by a fourth-order set of linear differential equations of the general form

$$\Delta\dot{x} = F\Delta x + G\Delta\delta \tag{1}$$

where the motion variables are contained in Δx,

$$\Delta x^T = (\Delta r \quad \Delta\beta \quad \Delta p \quad \Delta\phi) \tag{2}$$

and the control variables are

$$\Delta\delta^T = (\Delta\delta R \quad \Delta\delta A) \tag{3}$$

Stability derivatives, inertial effects, and kinematic relationships are contained in F. Neglecting unsteady aerodynamic effects, assuming that the flight path is horizontal, and considering only those aerodynamic side forces due to sideslip perturbation,

$$F = \begin{bmatrix} N_r & N_\beta & N_p & 0 \\ -1 & Y_\beta/V & 0 & g/V \\ L_r & L_\beta & L_p & 0 \\ 0 & 0 & 1 & 0 \end{bmatrix} \tag{4}$$

It is assumed that angles and angular rates are measured in stability axes, i.e., body axes which are nominally aligned with the velocity. The subscripted capital letters represent the sensitivities of specific forces and moments to state perturbations. The control effects matrix G is

$$G = \begin{bmatrix} N_{\delta R} & N_{\delta A} \\ 0 & 0 \\ L_{\delta R} & L_{\delta A} \\ 0 & 0 \end{bmatrix} \tag{5}$$

Defining Δr, $\Delta\beta$, and $\Delta\delta R$ as directional variables, and Δp, $\Delta\phi$, and $\Delta\delta A$ as lateral variables, both F and G can be partitioned as

$$\left[\begin{array}{l|l} \text{Directional effects} & \text{Lateral-to-directional coupling} \\ \hline \text{Directional-to-lateral coupling} & \text{Lateral effects} \end{array}\right]$$

$$F = \left[\begin{array}{c|c} F_D & F_L^D \\ \hline F_D^L & F_L \end{array}\right] \tag{6}$$

$$G = \left[\begin{array}{c|c} G_D & G_L^D \\ \hline G_D^L & G_L \end{array}\right] \tag{7}$$

The strength of lateral-directional coupling depends upon the relative magnitudes of the off-diagonal blocks. "Stability coupling," reflected in F, and "control coupling," defined by G, are distinctly separate phenomena; however, coupling in F almost certainly leads to coupled control response whether or not there is explicit coupling in G. Control coupling affects stability only when there is external feedback, provided either by pilot loop closures or the flight control system.

There are two circumstances in which lateral and directional dynamics can be considered separately, i.e., in which decoupled reduced-order models produce reasonable approximations to stability and response characteristics. If the off-diagonal blocks are negligibly small, the fourth-order model can be decoupled. Directional stability is defined by F_D, and lateral stability is defined by F_L. This is a limiting case in nonsingular perturbation analysis,[5,6] and the model reduction is referred to as "truncation."[4] If F_L^D and F_D^L are not small but the time scales of yawing and rolling motions are widely separated, and if the faster mode is stable, then reduced-order models can be generated by "residualization."[4] In this limiting case of singular perturbation analysis,[5,6] the slow mode behaves as if the fast mode is always in steady-state equilibrium, and the fast mode "sees" the slow mode as a gradually changing bias. The fast mode affects the stability of the slow mode, but the reverse effect is negligible. Related approximate modes can be found in Refs. 1 to 3.

Truncated Models

When the off-diagonal blocks are small, the Dutch roll motions are approximated by the directional equation,

$$\begin{bmatrix} \Delta\dot{r} \\ \Delta\dot{\beta} \end{bmatrix} = \begin{bmatrix} N_r & N_\beta \\ -1 & Y_\beta/V \end{bmatrix} \begin{bmatrix} \Delta r \\ \Delta\beta \end{bmatrix} + \begin{bmatrix} N_{\delta R} \\ 0 \end{bmatrix} \Delta\delta R \tag{8}$$

and the roll and spiral motions are derived from the lateral equation,

$$\begin{bmatrix} \Delta\dot{p} \\ \Delta\dot{\phi} \end{bmatrix} = \begin{bmatrix} L_p & 0 \\ 1 & 0 \end{bmatrix} \begin{bmatrix} \Delta p \\ \Delta\phi \end{bmatrix} + \begin{bmatrix} L_{\delta A} \\ 0 \end{bmatrix} \Delta\delta A \tag{9}$$

The roots of the corresponding second-order characteristic equations, $\Delta(s) = |sI - F| = 0$, govern the stability of the associated modes of motion. The Dutch roll natural frequency and damping ratio are approximated by

$$\omega_{n_{DR}} = (N_\beta + N_r Y_\beta/V)^{1/2} \tag{10}$$

$$\zeta_{DR} = -(N_r + Y_\beta/V)/2\omega_{n_{DR}} \tag{11}$$

The roll mode time constant is $-1/L_p$, and the spiral mode is neutrally stable, since its time constant is ∞. From Eq. (4), this approximation is seen to be reasonable when dihedral effect (L_β) is small and V is large.

Residualized Models

A system with fast and slow modes can be partitioned as

$$\begin{bmatrix} \Delta\dot{x}_S \\ \Delta\dot{x}_F \end{bmatrix} = \begin{bmatrix} F_S & F_F^S \\ F_S^F & F_F \end{bmatrix} \begin{bmatrix} \Delta x_S \\ \Delta x_F \end{bmatrix} + \begin{bmatrix} G_S & G_F^S \\ G_S^F & G_F \end{bmatrix} \begin{bmatrix} \Delta\delta_S \\ \Delta\delta_F \end{bmatrix} \tag{12}$$

The fast mode can be approximated by

$$\Delta\dot{x}_F = F_F\Delta x_F + F_S^F\Delta x_S + G_S^F\Delta\delta_S + G_F\Delta\delta_F \tag{13}$$

where the second term is a slowly changing bias. The slow mode solution assumes that Δx_F has reached the steady state, i.e., that $\Delta\dot{x}_F = 0$. The lower row of Eq. (12) is solved algebraically for Δx_F, and the result is substituted in the upper row of Eq. (12) to yield

$$\Delta\dot{x}_S = (F_S - F_F^S F_F^{-1} F_S^F)\Delta x_S + (G_S - F_F^S F_F^{-1} G_S^F)\Delta\delta_S - F_F^S F_F^{-1} G_F \Delta\delta_F \tag{14}$$

Three lateral-directional cases can be considered for residualization: 1) fast roll mode, neutral spiral mode, and slow Dutch roll mode; 2) fast roll mode, slow spiral mode, and slow Dutch roll mode; 3) slow lateral modes and fast directional mode.

In the first case, the roll angle can be neglected, and

$$\begin{bmatrix} F_S & F_F^S \\ F_S^F & F_F \end{bmatrix} = \left[\begin{array}{cc|c} N_r & N_\beta & N_p \\ -1 & Y_\beta/V & 0 \\ \hline L_r & L_\beta & L_p \end{array}\right] \tag{15}$$

Using Eqs. (13) and (14), the roll mode time constant is $-1/L_p$; the Dutch roll natural frequency and damping ratio are

$$\omega_{n_{DR}} = [N_\beta + N_r Y_\beta/V - (L_\beta + L_r Y_\beta/V) N_p/L_p]^{1/2} \tag{16}$$

$$\zeta_{DR} = -(N_r + Y_\beta/V - L_r N_p/L_p)/2\omega_{n_{DR}} \tag{17}$$

In the second case,

$$\begin{bmatrix} F_S & F_F^S \\ F_S^F & F_F \end{bmatrix} = \left[\begin{array}{ccc|c} N_r & N_\beta & 0 & N_p \\ -1 & Y_\beta/V & g/V & 0 \\ 0 & 0 & 0 & 1 \\ \hline L_r & L_\beta & 0 & L_p \end{array}\right]$$

The roll mode time constant is $-1/L_p$, while the Dutch roll and spiral mode characteristics are determined by the roots of the third-order characteristic equation,

$$\begin{aligned} \Delta(s) &= |sI - (F_S - F_F^S F_F^{-1} F_S^F)| \\ &= s^3 - (N_r - L_r N_p/L_p + Y_\beta/V)s^2 \\ &+ [(N_r - L_r N_p/L_p) Y_\beta/V + (g/V - N_p) L_\beta/L_p + N_\beta]s \\ &+ (L_r N_\beta - L_\beta N_r) g/VL_p = 0 \end{aligned} \tag{19}$$

When both roll and spiral motions are slower than directional motions,

$$\begin{bmatrix} F_S & F_F^S \\ F_S^F & F_F \end{bmatrix} = \begin{bmatrix} F_L & F_D^L \\ F_L^D & F_D \end{bmatrix} \tag{20}$$

Dutch roll characteristics are approximated by Eqs. (10) and (11), while roll-spiral modes are defined by

$$\Delta(s) = s^2 + c_1 s + c_0 = 0 \tag{21}$$

with

$$c_0 = (g/V)(L_\beta N_r - L_r N_\beta)/(N_\beta + N_r Y_\beta/V) \tag{22}$$

$$c_1 = -L_p + N_p (L_\beta + L_r Y_\beta/V)/(N_\beta + N_r Y_\beta/V) \tag{23}$$

The roots of this equation may be real or complex, stable or unstable, depending on the sizes and magnitudes of the stability derivatives. A coupled roll-spiral oscillation is predicted when $(c_1^2 - 4c_0) < 0$.

Stability Effects of Parameter Variations

Deterministic and stochastic sensitivity of the stability characteristics can be estimated using the reduced-order models, subject to the validity of the assumptions described above. Analytical expressions which predict the probability of instability are readily defined for low-order models using assumptions of linearity and decoupling. For high-order systems and parameter variations which exceed the linear region of the root-parameter relationship, a Monte Carlo computation of the sort described in a later section may be required.

Each eigenvalue, $\lambda_i = \alpha_i + j\omega_i$, $i = 1,\ldots,n$, can be written as a two-component real vector, $\lambda^T = [\alpha_i \omega_i]$, and it is a function of the characteristic equation coefficients c:

$$c^T = [c_0 \quad c_1 \ldots c_{n-2} \quad c_{n-1}] \tag{24}$$

Expanding in a Taylor series about the nominal coefficient values,

$$\lambda_i(c) = \lambda_i(c)\Big|_{c=c_0} + \frac{\partial \lambda_i}{\partial c}\Big|_{c=c_0} (c - c_0) + \cdots \tag{25}$$

The Jacobian matrix $\partial\lambda_i/\partial c$ is the sensitivity of the eigenvalue to variations in the coefficients. Similarly, c can be expressed as a function of the parameters p, which are the stability derivatives contained in Eq. (4):

$$p^T = [L_p \quad L_r \quad L_\beta \quad N_p \quad N_r \quad N_\beta \quad Y_\beta] \tag{26}$$

Expanding about the nominal parameter values,

$$c(p) = c(p)\Big|_{p=p_0} + \frac{\partial c}{\partial p}\Big|_{p=p_0} (p - p_0) + \cdots \tag{27}$$

where $\partial c/\partial p$ is the relevant Jacobian matrix. To first order, variations in the eigenvalue can be expressed as

$$\Delta\lambda_i = \frac{\partial \lambda_i}{\partial c}\Delta c = \frac{\partial \lambda_i}{\partial c}\frac{\partial c}{\partial p}\Delta p \tag{28}$$

Assuming that p is a Gaussian variable with mean p_0, the mean value of λ_i is

$$\bar{\lambda}_i = E\{\lambda_i[c(p)]\} = \lambda_i[c(p_0)] \tag{29}$$

where $E\{\cdot\}$ is the expectation operator.

The statistical variation of λ_i about its mean is represented by the covariance matrix Λ_i,

$$\Lambda_i = \begin{bmatrix} \sigma_{\alpha_i}^2 & \mu_i \sigma_{\alpha_i} \sigma_{\omega_i} \\ \mu_i \sigma_{\alpha_i} \sigma_{\omega_i} & \sigma_{\omega_i}^2 \end{bmatrix} \tag{30}$$

with standard deviation σ_{α_i} and σ_{ω_i} as well as a correlation coefficient μ_i. Defining the parameter covariance matrix as

$$P = E(\Delta p \Delta p^T) = \begin{bmatrix} \sigma_{L_p}^2 & \rho_{12}\sigma_{L_p}\sigma_{L_r} & \cdots & \cdot \\ \rho_{12}\sigma_{L_p}\sigma_{L_r} & \sigma_{L_r}^2 & \cdots & \cdot \\ \cdot & \cdot & \cdots & \cdot \\ \cdot & \cdot & \cdots & \sigma_{Y_\beta}^2 \end{bmatrix} \tag{31}$$

the eigenvalue covariance Λ_i can be written as

$$\Lambda_i = E(\Delta\lambda_i \Delta\lambda_i^T) = \frac{\partial \lambda_i}{\partial c}\frac{\partial c}{\partial p} P \frac{\partial c^T}{\partial p}\frac{\partial \lambda_i^T}{\partial c} \tag{32}$$

Equation (32) defines a "1-σ" ellipse about the mean eigenvalue, with principal axes skewed from the real and imaginary axes of the s-plane; the probability density function (pdf) of λ_i is

$$\text{pdf}(\lambda_i) = (2\pi|\Lambda_i|)^{-1/2} \exp[-\tfrac{1}{2}(\lambda_i - \bar{\lambda}_i)^T \Lambda_i^{-1} (\lambda_i - \bar{\lambda}_i)] \tag{33}$$

The probability of an instability in λ_i is found by integrating Eq. (35) over all λ and determining what portion of the integral lies in the right-half complex plane. If the coupling between real and imaginary variations in λ_i is negligible ($\mu_i \simeq 0$) or if λ_i is real, then the probability that λ_i will be driven to instability by parameter uncertainties is predicted by finding the value m for which

$$\alpha_i + m\sigma_{\alpha_i} = 0 \tag{34}$$

and referring to standard tables for scalar Gaussian density functions.[7] The probabilities associated with various degrees of instability, e.g., "times to double" of arbitrary value, are computed in similar fashion.

Numerical Example

Models of Space Shuttle Dynamics

Stability derivatives for the Space Shuttle flying at $M = 1.5$ on a return from orbit are derived from data in Ref. 8 and are given in Table 1. The mass of the vehicle is nominally 82,475 kg, corresponding to 181,450 lb, and the information is given in stability axes. I_{xx}, I_{zz}, and I_{xz} are approximately 7.8×10^5, 5.9×10^6, and 1.5×10^4 slug-ft^2, respectively.

The fourth-order Dutch roll and roll-spiral eigenvalues of Eq. (4) are compared with reduced-order eigenvalues in Table 2. (Values in parentheses are real roll and spiral roots.) The truncated Dutch roll model is seen to be a reasonable approximation of the fourth-order Dutch roll, but the truncated lateral model fails to predict the roll-spiral oscillation. As a consequence of low roll damping, the lateral mode is slower than the directional mode. Case 3, with truncated Dutch roll and residualized roll-spiral modes, captures the natural frequencies but underestimates the damping of both modes.

Further definition of the Space Shuttle's unaugmented dynamics is given by lateral-directional eigenvectors and transient response to an elevon step input. The eigenvector magnitudes, which are synonymous with the "time vector" magnitudes of Ref. 3, are listed in Table 3 and are normalized to the sideslip angle response. It can be seen that rolling response is dominant for both modes of motion. The Dutch roll's "ϕ/β" ratio is 8.7, and ϕ/β for the roll-spiral oscillation is ten times greater.

Roll response to aileron (or differential elevon) is the single most important lateral-directional control characteristic. The Space Shuttle has negative ("adverse") yaw response to elevon, indicating that the vehicle initially will yaw away from the commanded roll, causing a quasi-steady sidelip angle which "uncoordinates" the turn, as shown in Fig. 1. A 1-deg elevon deflection causes a quasi-steady roll rate of 4 deg/s which peaks after a lag of about 2 s. This is faster than the roll-mode time constant ($\tau_R = -1/\lambda_R$) predicted by the truncated model (Table 2), and strong modal coupling is apparent.

Aerodynamic Uncertainties and Simplified Estimates of Their Effects

In addition to aerodynamic coefficients, Ref. 8 provides estimates of 3-σ uncertainties and correlation coefficients for the static body-axis stability and control derivatives. These figures have been revised, but the preliminary values, shown in Table 4 as 1-σ values (i.e., one-third the original values), serve to demonstrate the analytical techniques presented here.

The dimensionless, body-axis coefficients are converted to dimensional, stability-axis derivatives in the conventional manner. For example, the roll- and yaw-moment effects of elevon are

$$\begin{bmatrix} L_{\delta A} \\ N_{\delta A} \end{bmatrix}_S = H_B^S I_B^{-1} \begin{bmatrix} C_{l_{\delta A}} \\ C_{n_{\delta A}} \end{bmatrix}_B \bar{q}Sb \tag{35}$$

The lateral-directional inertia matrix is

$$I_B = \begin{bmatrix} I_{xx} & -I_{xz} \\ -I_{xz} & I_{zz} \end{bmatrix} \tag{36}$$

and the body-to-stability-axis transformation is

$$H_B^S = \begin{bmatrix} \cos\alpha_0 & \sin\alpha_0 \\ -\sin\alpha_0 & \cos\alpha_0 \end{bmatrix} \tag{37}$$

Then the aileron roll-yaw uncertainty covariance matrix P transforms as

$$P_S = E\left\{ \begin{bmatrix} \Delta L_{\delta A} \\ \Delta N_{\delta A} \end{bmatrix}_S [\Delta L_{\delta A} \quad \Delta N_{\delta A}]_S \right\}$$
$$= (H_B^S I_B^{-1}) E\left\{ \begin{bmatrix} \Delta C_{l_{\delta A}} \\ \Delta C_{n_{\delta A}} \end{bmatrix}_B [\Delta C_{l_{\delta A}} \quad \Delta C_{n_{\delta A}}]_B \right\}$$
$$\times (\bar{q}Sb)^2 (H_B^S I_B^{-1})^T \tag{38}$$

where $\Delta(\ )$ connotes deviation from the mean value, and

$$E\left\{ \begin{bmatrix} \Delta C_{l_{\delta A}} \\ C_{n_{\delta A}} \end{bmatrix}_B [\Delta C_{l_{\delta A}} \Delta C_{n_{\delta A}}]_B \right\} = \begin{bmatrix} \sigma^2_{C_{l_{\delta A}}} & \rho\sigma_{C_{l_{\delta A}}}\sigma_{C_{n_{\delta A}}} \\ \rho\sigma_{C_{l_{\delta A}}}\sigma_{C_{n_{\delta A}}} & \sigma_{C_{n_{\delta A}}} \end{bmatrix} \tag{39}$$

Table 1 Lateral-directional stability derivatives of the Space Shuttle[a]

L_r	= 0.203	N_r	= −0.117	Y_β/V	= −0.090
L_β	= −5.003	N_β	= 0.587	$Y_{\delta R}/V$	= 0.008
L_p	= −0.490	N_p	= 0.053	$Y_{\delta A}/V$	= −0.002
$L_{\delta R}$	= 1.555	$N_{\delta R}$	= −0.594	g/V	= 0.023
$L_{\delta A}$	= 4.907	$N_{\delta A}$	= −0.397		

[a] Mach number = 1.5, dynamic pressure = 1120 kg/m^2 (230 psf), angle of attack = 6.6 deg.)

Table 3 Lateral-directional eigenvector magnitudes for the space shuttle example

	Dutch roll mode	Roll-spiral mode
Δr, deg/s	0.78	2.01
$\Delta\beta$, deg	1.	1.
Δp, deg/s	6.51	12.12
$\Delta\phi$, deg	8.7	87.5

Table 2 Comparison of lateral-directional eigenvalues of various Space Shuttle models

Model	$\omega_{n_{DR}}$, rad/s	ζ_{DR}	$\omega_{n_{RS}}(\lambda_R)$, rad/s	$\zeta_{RS}(\lambda_s)$, rad/s
Fourth-order	0.749	0.310	0.139	0.842
Truncated models	0.773	0.134	(−0.49)	(0.0)
Residualized model: Case 1	0.233	0.397	(−0.49)	(0.0)
Residualized model: Case 3	0.773	0.134	0.134	0.166

Table 4 Estimates of uncertainties in dimensionless body-axis aerodynamic derivatives[8]

Derivative	Value	1-σ uncertainty, % mean value	Correlation coefficient
C_{l_β}	−.0015	3.1	−.25
C_{n_β}	.00026	16.7	
$C_{l_{\delta A}}$	.0015	6.	+.24
$C_{n_{\delta A}}$	.00013	70.3	
$C_{l_{\delta R}}$	.0005	4.	−.3
$C_{n_{\delta R}}$	−.00087	5.2	

Table 5 Estimates of uncertainties in dimensional stability axis aerodynamic derivatives

Derivative	1-σ uncertainty, % mean value	Correlation coefficient
L_β	3.1	−.82
N_β	4.	
$L_{\delta A}$	6.	−.64
$N_{\delta A}$	7.9	
$L_{\delta R}$	5.9	−.73
$N_{\delta R}$	4.5	

Estimates of stability-axis derivatives based on Table 4 are shown in Table 5. In spite of the rather large percentage uncertainties in body-axis C_{n_β} and $C_{n_{\delta A}}$, the net uncertainties in stability-axis N_β and $N_{\delta A}$ are of the same order as the remaining uncertainties. This is largely an effect of the product of inertia, I_{xz}, in Eqs. (36) and (38) and the overriding coupling of body-axis roll moments into stability-axis yaw moments. Uncertainties for the remaining lateral-directional derivatives are not presented in Ref. 8; hence, the example uses an average value of 5.2% for 1-σ uncertainties in side-force and rotary derivatives. Together with Table 5, they are used to define the parameter covariance matrix P [Eq. (31)]. Although the correlations are not small (Table 5), they are neglected for simplicity below.

Standard deviations of Dutch roll and roll-spiral mode total damping ($\alpha_i = -\zeta\omega_{n_i}$) are estimated by applying Eq. (32) to the truncated and residualized models, Eqs. (8) and (20), using the data contained in Tables 1, 2, and 5. The value of m required for neutral stability [Eq. (34)] is calculated using the fourth-order eigenvalues as bases. For the Dutch roll mode, σ_α is 0.0089, and $\zeta\omega_n = 0.232$; hence, $m = 26.1$, and there is virtually no chance that parameter variation will drive this mode to instability. For the roll-spiral oscillation, $\sigma_\alpha = 0.0205$, $\zeta\omega_n = 0.117$, and $m = 5.7$. A $+5.7$-σ parameter variation would cause instability, but the probability of this occurring is considerably less than 0.0001. Examining the contributions of individual parameter uncertainties to the roll-spiral σ_α, the four most significant terms are ranked as follows: σ_{L_p}, σ_{n_p}, σ_{n_β}, and σ_{L_β}.

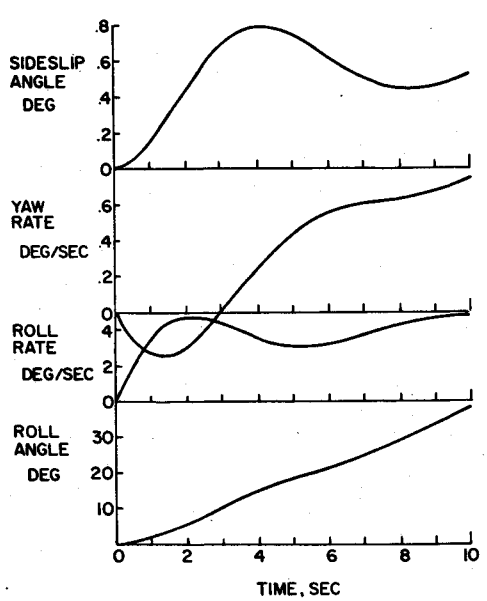

Fig. 1 Response to 1-deg differential elevon step input.

Flight Control System Models

The Space Shuttle's Early- and Late-Entry Digital Flight Control Systems[9] have been simplified and modeled as continuous-time ("analog") systems for analysis. Reaction control logic and structural-mode filters are eliminated, gains are held at constant values, and nonlinearities are linearized. The Early-Entry FCS (EFCS) shown in Fig. 2 uses rudder and reaction control thrusters to command stability-axis bank angle through kinematics, sideslip angle, and dihedral effect. With staged firing of thrusters, the reaction control logic approximates a quantized linear control moment which can be modeled, over a limited range, by increased values of $N_{\delta R}$. Lateral hand controller inputs, $\Delta\delta S$, are pre-filtered and subjected to proportional-integral compensation. The final low-pass filters prior to rudder and elevon commands, $\Delta\delta R_c$ and $\Delta\delta A_c$, are used to aggregate the effects of actuation delay and rate limiting, with nominal bandwidths of 10 rad/s. Turn coordination is provided by $(\Delta r - \Delta\phi g/V)$ feedback to controls. The EFCS adds four states to the closed-loop dynamic model described by Eq. (4); these correspond to the three low-pass filters and integral compensation.

The Late-Entry FCS (LFCS) shown in Fig. 3 uses differential elevons in conventional fashion, and it incorporates an aileron-rudder interconnect to account for adverse aileron yaw. There is proportional-integral compensation for both control surfaces, and the foot pedals, $\Delta\delta P$, are enabled to aid turn coordination. Actuator delays are treated in the same way as above. The LFCS adds six states to the closed-loop dynamic model. The lateral acceleration feedback, Δa_y, is modeled as $Y_\beta \Delta_\beta$ for analysis. Additional details of the EFCS and LFCS models can be found in Ref. 10.

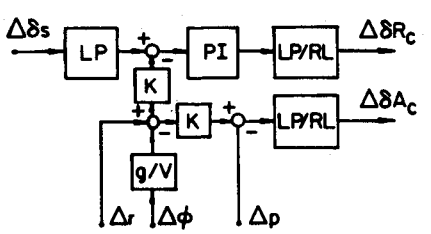

Fig. 2 Simplified model of Early-Entry Flight Control System (EFCS): LP = low-pass filter, PI = proportional-integral compensation, RL = rate limiter, K = gain.

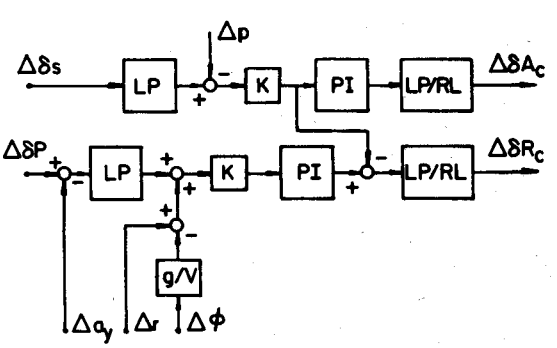

Fig. 3 Simplified model of Late-Entry Flight Control System (LFCS).

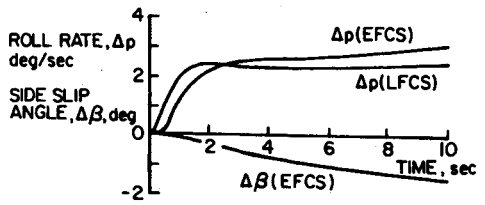

Fig. 4 Responses to lateral hand controller step input with Early-Entry and Late-Entry Flight Control Systems.

With nominal aerodynamic coefficients, both control modes provide substantial flying qualities improvements, as can be seen by comparing the lateral hand controller responses of Fig. 4 with Fig. 1. Roll rate response is essentially deadbeat, although the EFCS allows a slow increase that results from decreasing sideslip angle and negative dihedral effect. Sideslip response with the LFCS is two orders of magnitude smaller, allowing nearly ideal roll response.

The classical response modes described earlier are strongly affected by the flight control systems, as portrayed by the closed-loop eigenvalues and eigenvectors. Table 6 presents the Space Shuttle/EFCS eigenvalues together with the largest and next largest components of the corresponding eigenvectors. All modes are stable. The four lowest frequency modes are associated with the vehicle's rigid-body dynamics, while the faster modes involve the input and control surface states through EFCS dynamics. The first and fourth modes can be identified as spiral and roll modes, respectively, and there is no perceptible Dutch roll oscillation.

Table 7 presents similar information for the LFCS. The first (spiral) mode is essentially neutral, and the fourth (roll) mode is about twice as fast as the EFCS roll mode. The third mode is the Dutch roll, and the control system variables are dominant in four LFCS modes.

Thus it appears that Space Shuttle flying qualities benefit from the EFCS and LFCS when aerodynamic parameters are as predicted; however, the classical rigid-body modes can not be identified by their eigenvalues alone, and are difficult to identify from the eigenvectors. This poses a severe problem for the definition and application of parameter-based flying qualities criteria; results such as Fig. 4 suggest that analysis problems can be alleviated by using response-oriented criteria.

Table 6 Space shuttle eigenvalues and eigenvectors with the early-entry flight control system

$\omega_n(\lambda)$, rad/s	ζ	Largest component	Second largest component
(−0.0007)	···	Roll angle	Yaw rate
(−0.062)	···	Roll angle	Roll rate
(−0.351)	···	Roll angle	Roll rate
(−1.277)	···	Roll rate	Roll angle
(−5.)	···	Command input	Elevon
(−8.647)	···	Rudder	Elevon
10.32	0.502	Elevon	Roll rate

Table 7 Space shuttle eigenvalues and eigenvectors with the late-entry flight control system

$\omega_n(\lambda)$, rad/s	ζ	Largest component	Second largest component
$(+2.6\times10^{-5})$	···	Roll angle	Yaw rate
0.166	0.924	Roll angle	Rudder integrator
2.164	0.552	Rudder	Roll rate
(−2.641)	···	Roll rate	Rudder
(−5.)	···	Elevon	Roll rate
(−5.877)	···	Elevon	Rudder
7.575	0.956	Rudder	Elevon

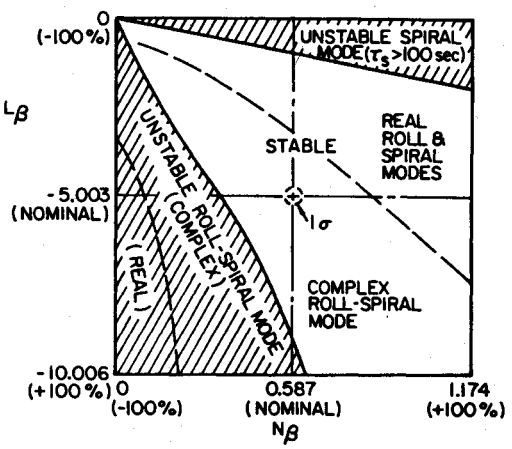

Fig. 5 Effects of L_β and N_β variations on Space Shuttle stability, no FCS.

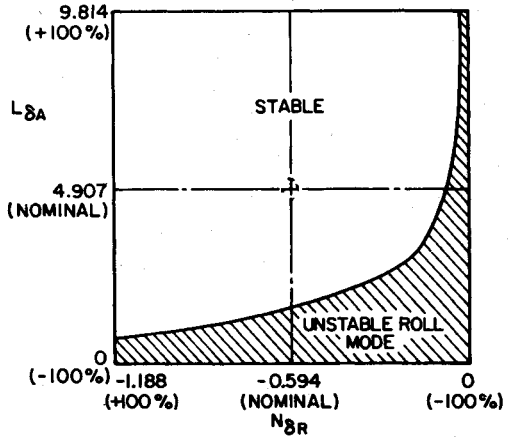

Fig. 6 Effects of $L_{\delta A}$ and $N_{\delta R}$ on Space Shuttle stability, early-entry FCS.

Effects of Parameter Variations

Deterministic Stability Boundaries

Deterministic stability boundaries for open- and closed-loop models are defined by varying the aerodynamic derivatives, computing the eigenvalues, and cross-plotting to define the regions of stability and instability as functions of the derivatives. This approach identifies the percentage variation needed to cause instability, but it gives no indication of the probability of exceeding a stability boundary.

L_β and N_β variations of ±100% affect unaugmented airframe stability as presented in Fig. 5. Flying qualities improve as N_β increases and L_β decreases, with separate roll and spiral modes reappearing for variations of 30% to 40% in either variable. The roll-spiral mode is driven to instability by comparable variations of opposite sign.

Although not shown, L_p and N_p variations of −45% and +30% induce an unstable roll-spiral mode, while N_r must increase by 80% to cause a spiral instability. Combining −90% N_p variation with +90% N_r variation causes Dutch roll instability. No instabilities are caused by ±100% variations of L_r.

With a minor exception, ±100% variations in these six stability derivatives introduce no new instabilities when either the EFCS or LFCS is engaged. The EFCS has an unstable roll-spiral mode when N_β has dropped to zero and L_β is doubled. The two control systems provide from 5 to 20 times the damping of the unaugmented vehicle; hence, 100% variations in L_p, L_r, N_p, and N_r have negligible effect.[10] However, the reduced sensitivity to stability-derivative variations is ac-

Table 8 Probability of instability due to aerodynamic variations

	Percentage of cases in given range						
	τ(stable), s			$-\tau$(unstable), s			
Case (no. of trials)	5-10	10-100	100-∞	∞-100	100-20	20-10	10-8
FCS off (1000)	70	30	...	...	...	...	...
EFCS[a] (1000)	...	...	100	...	...	...	...
LFCS[a] (1000)	...	...	42	58	...	...	...
EFCS[b] (100)	...	...	100	...	...	...	...
LFCS[b] (100)	...	...	...	1	9	55	35

[a] Actuator bandwidth = 10 rad/s. [b] Actuator bandwidth = 1 rad/s.

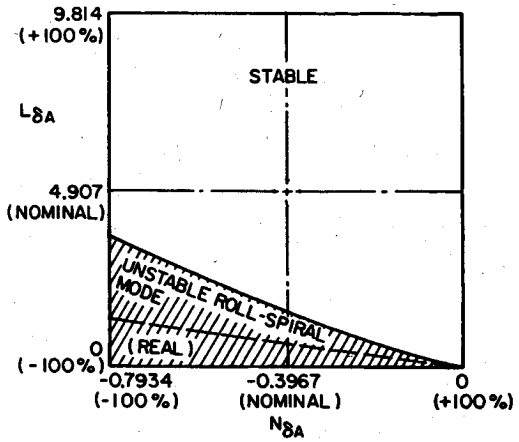

Fig. 7 Effects of $L_{\delta A}$ and $N_{\delta A}$ on Space Shuttle stability, early-entry FCS.

companied by increased sensitivity to control-derivative variations.

Figure 6 illustrates the effects of variations in the main control derivatives $L_{\delta A}$ and $N_{\delta R}$ on closed-loop EFCS stability. The roll mode instability which results is potentially severe, with unstable time constants less than 0.5 s. A plot for the LFCS has similar shape, but the late-entry system has greater tolerance to $L_{\delta A}$ variations and lower tolerance to $N_{\delta A}$ variations.

Increased values of $L_{\delta R}$ in combination with 70% to 90% reductions in $N_{\delta R}$ lead to roll instability for both control systems. The EFCS develops very long period spiral instability for variations of opposite sign. The standard deviations of $L_{\delta R}$ and $N_{\delta A}$ are about 5% of nominal values, so there is little chance of instability.

The combined effects of $L_{\delta A}$ and $N_{\delta A}$ variations are shown in Fig. 7 for the early-entry FCS case. The unstable roll-spiral boundary indicated in Fig. 7 for low values of $L_{\delta A}$ is very sensitive to elevon yaw ($N_{\delta A}$). More negative values of $N_{\delta A}$ lead to instability for smaller $L_{\delta A}$ variations.

Monte Carlo Stability Analysis

An alternative approach for evaluating the probability of instability is to conduct a numerical experiment in which the parameters are varied by a random number generator (subject to the means and standard deviations specified in Tables 1 and 5), the eigenvalues are computed, and statistics of the eigenvalues are compiled. The computations are repeated a large number of times in this Monte Carlo stability analysis, with all stability and control derivatives being varied on every trial. This procedure has the advantage that it does not require linear root sensitivity, roots are free to change from real to complex (or back), high-order models can be tested, correlations can be considered easily, and the random trials are readily implemented, given the basic routines for eigenvalue computation. The principal disadvantage is that a large number of trials may be required for statistical confidence.

In the present example, the stability assessment is based on the real part α of the least stable eigenvalue. A cumulative distribution of the number of trials in which α is greater than selected values provides an estimate of the actual probability distribution. Correlations are neglected to facilitate comparisons with earlier results. Table 8 summarizes results for several open- and closed-loop cases.

All 1000 trials for both the unaugmented vehicle and the EFCS are stable, with least stable time constants of 5 s or more. Seventy percent of the unaugmented vehicle's least stable eigenvalues have time constants between 5 and 10 s, and the remaining 30% fall between 10 and 100 s. These results are consistent with the simplified analysis. All of the EFCS's least stable time constants fall between 100 s and infinity.

Over half (58%) of the LFCS's least stable roots are unstable, but their time constants range between infinity and 100 s and pose no threat to flying qualities. The remaining 42% are fully stable, with least stable time constants of 100 s to infinity.

These results assume an actuation bandwidth of 10 rad/s, as determined by the output low-pass filters in Figs. 2 and 3. A number of factors could reduce the effective actuation bandwidth, most notably computation lags, transmission delays, and rate limiting. Actuation bandwidth has no effect on EFCS stability, but large delays and rate limiting can drive the simplified LFCS model to instability.

With bandwidth reduced to 1 rad/s, all EFCS cases remain stable, and a further reduction to 0.1 rad/s does not change this result. With 1 rad/s bandwidth, 90% of the LFCS cases have a root whose unstable time constant is -20 s or more, and 35% have time constants of -8 to -10 s. Increasing the bandwidth to 2 rad/s restores stability; in fact, there are fewer unstable cases than in the nominal case. Further investigation reveals that rudder lags have statistically greater destabilizing effect than elevon lags.

Conclusion

Models for examining the effects of aerodynamic parameter variations on lateral-directional stability have been developed and applied to a Space Shuttle example. Conditions for using truncated and residualized reduced-order models are presented, and their utility for characterizing eigenvalue sensitivity is shown. Covariance analysis is used to predict the probability of instability with these simple models. The probability of instability in higher-order dynamic systems, as introduced by flight control compensation, is evaluated by Monte Carlo computation of eigenvalues, a computer-intensive but general approach. With assumed values of parameter uncertainty, the example's stability is found to be relatively tolerant to variations in aerodynamic derivatives. Feedback control provides insensitivity to stability derivative variations, but "tight" control increases sensitivity to control derivative variations; hence, the probability of instability due to uncertainties in control effects is heightened in this example.

Acknowledgments

This research was sponsored in part by NASA Langley Research Center under Contract No. NAS1-13502.

References

[1] Seckel, E., *Stability and Control of Airplanes and Helicopters,* Academic Press, New York, 1964.

[2] Etkin, B., *Dynamics of Atmospheric Flight,* Wiley, New York, 1972.

[3] McRuer, D., Ashkenas, I., and Graham, D., *Aircraft Dynamics and Automatic Control,* Princeton University Press, Princeton, N.J., 1973.

[4] Harvey, C.A., and Pope, R.E., "Study of Synthesis Techniques for Insensitive Aircraft Control Systems," NASA CR-2803, April 1977.

[5] Nayfeh, A., *Perturbation Methods,* Wiley, New York, 1973.

[6] Sandell, N.R., Jr., Varaiya, P., Athans, M., and Safonov, M.G., "Survey of Decentralized Control Methods for Large Scale Systems," *IEEE Transactions on Automatic Control,* Vol. AC-23, No. 2, April 1978, pp. 108-128.

[7] Hodgman, C.D. (ed.), *C.R.C. Standard Mathematical Tables,* Chemical Rubber Publishing Co., Cleveland, 1963.

[8] "Aerodynamic Design Data Book, Volume I, Orbiter Vehicle," Rockwell SD 72-SH-0060-IJ, Dec. 1975.

[9] "Space Shuttle Orbital Flight Test, Level C, Functional Subsystem Software Requirements; Guidance, Navigation, and Control; Part C: Flight Control-Entry," Rockwell International, Downey, Calif., Nov. 1976.

[10] Stengel, R.F., and Miller, G.E., "Flying Qualities of an Aircraft with Strong Lateral-Directional Coupling," NASA CR-158961, Dec. 1978.